

Available online at www.sciencedirect.com**ScienceDirect**journal homepage: www.elsevier.com/locate/issn/15375110**Research Paper****Automatic detection of curved and straight crop rows from images in maize fields**

Iván D. García-Santillán ^{a,b,*}, Martín Montalvo ^a, José M. Guerrero ^a, Gonzalo Pajares ^a

^a Department of Software Engineering and Artificial Intelligence, Faculty of Informatics, Complutense University, Madrid, Spain

^b Department of Software Engineering, Universidad Técnica del Norte, Ibarra, Ecuador

ARTICLE INFO**Article history:**

Received 29 February 2016

Received in revised form

28 September 2016

Accepted 27 January 2017

Keywords:

Automatic guidance

Crop row detection

Image segmentation

Machine vision

Hough transform

A new method for detecting curved and straight crop rows in images captured in maize fields during the initial growth stages of crop and weed plants is proposed. The images were obtained under perspective projection with a camera installed on board and conveniently arranged at the front part of a tractor. The final goal is the identification of the crop rows with two purposes: a) precise autonomous guidance; b) site-specific treatments, including weed removal, where weeds are identified as plants outside the crop rows. Image quality is affected by uncontrolled lighting conditions in outdoor agricultural environments and gaps along the crop rows due to lack of germination or defects during planting. Also, different crop and weed plant heights and volumes appear at different growth stages affecting the crop row detection process. The proposed method was designed with the required robustness to cope with the above situations and consists of three linked phases: (i) image segmentation, (ii) identification of starting points for determining the beginning of the crop rows and (iii) crop rows detection. The main contribution of the method is the ability to detect curved and straight crop rows having regular or irregular inter-row spacing, even when both row types coexist in the same field and image. The performance of the proposed approach was quantitatively compared against six existing strategies, achieving accuracies between 86.3% and 92.8%, depending on whether crop rows were straight/curved with regular or irregular spacing, with processing times less than 0.64 s per image.

© 2017 IAgE. Published by Elsevier Ltd. All rights reserved.

* Corresponding author. Department of Software Engineering and Artificial Intelligence, Faculty of Informatics, Complutense University, Madrid, Spain.

E-mail addresses: ivandgar@ucm.es (I.D. García-Santillán), mmontalvo@fdi.ucm.es (M. Montalvo), jmguerre@ucm.es (J.M. Guerrero), pajares@ucm.es (G. Pajares).

<http://dx.doi.org/10.1016/j.biosystemseng.2017.01.013>

1537-5110/© 2017 IAgE. Published by Elsevier Ltd. All rights reserved.

Nomenclature	
Abbreviations	
CRD	crop row detection
CRDA	crop row detection accuracy
CRDA*	slight variant of CRDA
DAGP	detection by accumulation of green pixels
DBMR	detection based on micro-ROIs
ExG	excess green
GNSS	global navigation satellite systems
GPS	global positioning system
HT	Hough transform
LRQ	linear regression based on least squares
LTS	linear regression based on the Theil-Shen estimator
RHEA	robotics and associated high-technologies and equipment for agriculture and forestry
ROI	region of interest
RTK-GPS	real time kinematics-global positioning system
TMGEM	template matching followed by global energy minimisation
Symbols	
A	number of white pixels
a, b, c	coefficients for the quadratic polynomial
A _{sampled}	sampled area
A _{weed}	area covered by weeds
h	number of experimental and predicted equations
m, d	slope and intercept of the straight line respectively
M	number of image rows
N	number of crop rows
P _n	centroid (geometric centre) located in the n-th strip, $n = 1, \dots, 12$
P(i, j)	points at curved crop rows with (i, j) pixels coordinates
$\hat{P}(i, \text{columns} - j + 1)$	translated points from P(i, j), columns = 2000
Q	vector of parameters to be estimated
r, g, b	chromatic co-ordinates
R, G, B	RGB (red, green and blue) spectral channels
R _{max} , G _{max} , B _{max}	maximum values in the spectral channels
R _n , G _n , B _n	normalised RGB spectral channels
Rs	norm of residues
s	inter-row space in pixels
v	number of experimental and predicted values
(x, y)	upper left corner co-ordinates of the micro-ROI
(\bar{x}, \bar{y})	geometric centre of the micro-ROI
(x _c , y _c)	co-ordinates of the centroid
(X _{cross} , Y _{cross})	crossing point defining two rows intersecting
x _i , \hat{x}_i	experimental and predicted values at the i-th point, $i = 1, \dots, v$
Z	vector of measured data
Greek symbols	
ϵ_i (Q, Z)	error between the model (Q) and data (Z) at the i-th equation, $i = 1, \dots, h$
ρ	distance of the straight line at the origin in polar co-ordinates
θ	angle that forms the normal with the x-axis in polar co-ordinates

1. Introduction

1.1. Problem statement

Machine vision systems applied to agricultural tasks have great potential, as explained in Brosnan and Sun (2002) and Davies (2009). The use of technology, including vision systems, in agricultural applications can reduce manual tasks and the cost of crop production (Barreda, Ruiz, & Ribeiro, 2009), and can contribute to the productivity and competitiveness of farmers to ensure agricultural supplies. Moreover, the use of traditional farming methods may lead to indiscriminate use of chemicals (herbicides, fertilisers), increasing production costs, soil depletion and environmental pollution (Astrand & Baerveldt, 2005; Kataoka, Kaneko, Okamoto, & Hata, 2003).

Process automation is gaining an important relevance today. In this regard, crop rows detection in wide row crops is an important issue for both weed identification and automatic guidance. Indeed, plants located inside the inter-row spaces can be considered with very high probability to be weeds, requiring site-specific treatments (Emmi, Gonzalez-de-Soto, Pajares, & Gonzalez-de-Santos, 2014; RHEA, 2014). In autonomous tractors, navigation is mainly based on RTK-GPS (real time kinematics-global positioning system) consisting of two GNSS (global navigation satellite systems) rover antennas

providing localisation errors of below ± 20 mm (Emmi et al., 2014) for precise guidance. Nevertheless, when small deviations occur with RTK-GPS, crop rows detection is used for precise correction (Kise & Zhang, 2008; Rovira-Más, Zhang, Reid, & Will, 2003). This paper is devoted to automatic crop row detection in maize fields based on a machine vision system.

Outdoor agricultural environments are affected by uncontrolled, variable lighting conditions (sudden shadows, excessive or poor illumination) affecting the image quality. Additionally, different scene conditions can complicate precise crop row detection leading to errors in the estimation of row width from images: a) shortage of crop plants, due to lack of germination, defects during planting or pests/disease; b) high weed density with similar spectral signature to crops close to the crop row; c) different plant heights and volumes, due to different growth stages, are mapped under image perspective projection with different widths; d) curved terrain side slopes, movements of the tractor in irregular terrains, produce the mapping (under perspective projection) of points on the scene into unexpected positions on the image.

In the Andean region of Ecuador, where the present study was carried out, topography is hilly with significant slopes and curved crop rows on terraces are the norm. Terraces are used to avoid soil erosion of agricultural fields caused by natural and artificial irrigation. Curved crop rows also appear in flat parcels of lands with irregular geometry.

Several solutions have been proposed to cope with the above adverse situations with the aim of crop row detection (Hague, Tillett, & Wheeler, 2006; Ribeiro, Fernandez-Quintanilla, Barroso, & Garcia-Alegre, 2005; Vidović, Cupec, & Hocenski, 2016). However, because of the intrinsic difficulty involved in outdoor agricultural environments, further research is required to improve the detection of curved crop rows. According to the above considerations, a new global strategy was designed for detecting both straight and curved crop rows spaced 0.85 m, with variations ranging from 0.75 m to 0.95 m, under the above mentioned adverse environmental conditions.

The proposed strategy exploits the performance of some partial image-based procedures involved in existing methods and includes new procedures to achieve a valid methodology for crop row detection under different types of crop row alignments.

1.2. Review of methods

a) Hough Transform

Hough Transform (HT) can be used for crop rows detection when they are uniformly distributed across a field with weeds irregularly on the inter-row spaces, but with low densities. Rows are shown in maximum peaks in Hough space. Astrand and Baerveldt (2005) used the HT in fields of sugar beet by using a greyscale camera with a filter close to infrared. Barreda et al. (2009) fitted the crop rows based on the calculated vanishing point. Leemans and Destain (2006) applied previous knowledge with respect to crop rows position and direction in order to restrict the search in the Hough space. Gée, Bossu, Jones, and Truchetet (2008) applied a double HT.

b) Linear Regression

Sogaard and Olsen (2003) located crop rows in barley by using weighted linear regression. Hague et al. (2006) predicted position and orientation of the crop rows by applying the extended Kalman filter. Montalvo et al. (2012) and Guerrero et al. (2013) developed specific methods for maize fields. The first study used a template (binary mask) to determine the limits of the expected crop rows. The second approach applied prediction about the expected position of the crop rows and then were adjusted through the Theil-Sen estimator.

c) Blob analysis

The images are segmented based on blobs or clusters of pixels belonging to crops. The gravity centres of these clusters determine straight rows, allowing the association of an equation with each crop row. Based on these associations and considering the direction and displacement of the tractor, crop rows were detected (Bengochea-Guevara, Conesa-Muñoz, & Ribeiro, 2012; Burgos-Artizru, Ribeiro, Guijarro, & Pajares, 2011). Jiang, Wang, and Liu (2015) presented an algorithm based on multi-ROIs (small regions of interest, ROI) and least squares fitting, given a known inter-row space in fields of wheat, corn and soybean. Fontaine and Crowe (2006) grouped adjacent pixels in blobs with more than 200 pixels by applying

the criterion of grey level similarity, where the angle of the main axis and the gravity centre of each blob were obtained, which determine straight rows, i.e. the crop rows.

d) Alignments of green pixels

Parallel straight crop rows in the 3D scene, under perspective projection with the pinhole camera model, are imaged intersecting at a point called vanish point and only these rows are considered in the image. Jiang, Wang, Wang, and Liu (2016) combined the vanishing point constraint with the HT. Romeo et al. (2012) applied a method to identify straight crop rows in maize fields by exploring accumulation of green pixels along lines that converge on the vanishing point. Vidović et al. (2016) applied the vanishing point principle to determine that parallel crop rows (straight and curved) are imaged preserving the inter-crop row distances (regular patterns), which allows to apply a matching technique to combine image evidence and prior knowledge about the geometric structure. Optimisation, based on dynamic programming, was applied for straight and curved crop row detection for different row crop (maize, celery, potato, onion, sunflower and soybean) and growth stages. García-Santillán, Guerrero, Montalvo, and Pajares (2017) proposed a crop row detection approach with exhaustive exploration of pixels' alignments based on accumulation of green pixels, which are fitted by parabolas or straight lines. This method does not require the vanishing point assumption.

e) Frequency Analysis

These methods assume that parallel crop rows in the 3D scene show specific features and patterns after filtering. Bossu, Gée, Jones, and Truchetet (2009) applied wavelet transform in spatial domain, while Hague and Tillett (2001) applied band-pass filtering in the frequency domain.

f) Stereo Vision

These methods are usually used if the heights of weed and crop plants above ground are significant and if weed and crop plants differ in height (Romeo et al., 2012). Kise and Zhang (2008) determined 3D locations belonging to objects of interest in the scene, which were imaged as elevation maps for crop row detection to guide the tractor. Rovira-Más, Zhang, and Reid (2008) built 3D maps by combining the captured information provided by a stereo vision system, a location sensor and an inertial measurement unit for monitoring and automatic navigation.

After the review of methods, it was concluded that most approaches are not suitable for solving the problem of detecting both, curved and straight crop rows with regular or irregular inter-crop row spacing. Nevertheless, they have provided useful insights which are exploited to design the proposed method, which are the following: a) the HT in piecewise straight lines in order to determine starting points to find crop rows with possible curvature; b) least squares for fitting polynomial (linear or quadratic) parameters defining the adjusted crop rows and c) multi-ROIs in green pixel accumulations and blob analysis to find interest points along the crop rows.

2. Materials and methods

2.1. Image collection

The images used in this study were captured during February and March 2015 on an experimental field of maize at the San Francisco Research Station, Tulcán-Ecuador, located 2787 m above sea level (Latitude 0.62°N and Longitude –77.75°W), covering an area of 2 ha. The terrain is irregular with slopes of up to 12°. Acquisitions were spaced six days apart over a period of 40 d in order to obtain images under different environmental lighting conditions and different growth stages of maize and weed plants. Additionally, several images coming from the RHEA (2014) project containing straight crop rows of maize fields were also processed. These images were also captured on different days spaced 4–5 days apart over periods of 40 days in May and June during years 2012–2014, to obtain images under different conditions. Figure 1 shows illustrative examples of the images captured on the field with maize crops having certain features, such as: number of leaves in the range [4, 6], plant heights between 100 and 300 mm and plant population about 40,000 plants per ha. In (a) crop with a low presence of weeds, in (b) different shadows are projected on the ground, increasing the degree of difficulty for the image processing with respect to the greenness extraction, (c) different sizes of maize plants and presence of gaps, with lengths up to 1.20 m in the same crop row. The gaps are produced by errors during the sowing or perhaps because the maize seeds have not yet emerged. Furthermore, examples of images acquired under different lighting conditions are shown for (d) a sunny day with high level of illumination with

a certain tendency to image saturation, (e) a cloudy day where the illumination is considerably reduced, (f) a day with intermediate illumination levels with respect the two former. The crop rows were spaced 0.85 m, with variations ranging from 0.75 m to 0.95 m, particularly in curved crop rows.

The images from the maize fields in Ecuador were obtained with a GoPro Hero 3+ Black Edition colour camera, model CHDHX-302, (GoPro Inc. San Mateo CA, USA), which is equipped with an image sensor size 42 mm, pixel size 1.55 µm and focal length of 3 mm. The camera was mounted on the front of a New Holland TD90 tractor moving at an average speed of 3 km h⁻¹ (0.83 ms⁻¹). The machine vision system arrangement on board the tractor was established at a height of 2 m from the ground and with the optical axis inclined 45° with respect to the ground (pitch angle) and without lateral displacements (i.e. with roll and yaw angles set to 0°). This arrangement together with the focal length and sensor resolution permit the determination of the correspondence of distances and areas in the 3D original scene to pixels on the 2D image by applying a simple transformation between coordinate systems.

The digital images were captured under perspective projection and stored as 24-bit colour images with resolutions of 3000 × 2250 pixels (7 Mpx) saved in RGB colour space in JPG format. Nevertheless, only a reduced area on the ground is of interest either for applying site-specific treatments or as reference for guiding, denoted the Region of Interest (ROI). The size and location of the ROI must be specified considering (i) the number of crop rows to be detected and (ii) the imaged ROI that contains enough resolution (in pixels) to identify unambiguously green plants (crop and weed) from soil and also with



Fig. 1 – Illustrations of images processed by the method on maize crops with certain features: number of leaves in the range [4, 6], plant heights between 100 and 300 mm and plant population about 40,000 plants per ha. (a) Crop with a low level of weed; (b) presence of shade; (c) presence of gaps and plants of different sizes. Images acquired under different lighting conditions: (d) sunny day; (e) cloudy day; (f) intermediate day.

sufficient points to estimate the equations that define the crop rows. In the proposed approach four crop rows were selected for detection, in the same as reported by Emmi et al. (2014) for the RHEA (2014) project because the implements had four pairs of burners for weed control, each pair acting on a crop row. Considering the four crop rows and the inter-row space of 0.85 m the total width of the ROI is 3.4 m, which is fixed independently of the variations of the crop spacing. This area starts at 3 m ahead with respect to a virtual vertical axis traversing the centre of the image plane in the camera. This value avoids that the elements in front of the tractor are imaged. The length in the scene along the row was fixed to 5 m because it provides sufficient image resolutions as explained above. Figure 2(a) shows the ROI enclosed in the rectangle indicating the measures. This 3D area in the field results in an image resolution of 2000×650 pixels (width \times length), which represents approximately 20% of the full original image and is always located at the same position inside the image. Nevertheless, the method can be easily adapted for detecting any number of crop rows given a suitable camera configuration.

The images from the GoPro Hero 3+ belong to sequences of images captured with the tractor moving forward at a constant and previously fixed speed (set to 3 km h^{-1}), requiring 6 s to travel along the 5 m length of the ROI. The camera captures images at 2 fps, so that frames without overlap in the same ROI are spaced 12 frames apart. Accordingly, frames 12 units apart in a video sequence were processed. If a frame had to be discarded (because no crop rows are detected due to the problems that will be described later), the next frame in the sequence was selected, and so on, unless all frames captured during the time-window of 6 s (discounting the 637 ms required for processing an individual image according to Table 4) were discarded.

Table 2 – CRDA for tests on curved crop rows equally spaced.

CRDA	SET-2		
	TMGEM	DAGP	DBMR
Average	0.871	0.863	0.903
Skewness	-0.911	-2.064	-0.769
Kurtosis	4.141	4.311	3.410
Rank (with average)	2	3	1

Table 3 – CRDA* (slight variant of CRDA) for tests on curved crop rows non-equally spaced.

CRDA*	SET-3		
	TMGEM	DAGP	DBMR
Average	0.548	0.856	0.863
Skewness	-1.154	-1.867	-0.911
Kurtosis	4.499	4.467	3.712
Rank (with average)	3	2	1

Table 4 – Average execution times in percentage (%) and milliseconds (ms) for each module of the DBMR (Detection based on micro-ROIs).

Modules	Percentage (%)	Test-1 (ms)	Test-2 (ms)	Test-3 (ms)
1 Segmentation	41.7	239	255	265
2 Identification of starting points	8.8	50	54	57
3 Crop rows detection	49.6	284	304	315
Total	100	573	612	637

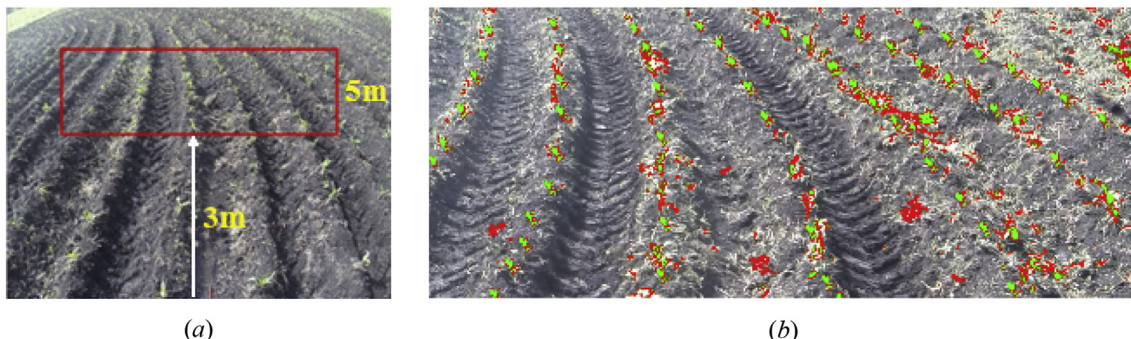


Fig. 2 – (a) Location of the ROI in the original RGB image as a red rectangle (2000×650 pixels); (b) identification of the soil (grey), weed (red) and crop (green) in the ROI.

Table 1 – Crop Row Detection Accuracy (CRDA) for tests on straight crop rows. CRDA values can range between 0 and 1 where a higher score indicates better performance.

CRDA	SET-1					
	HT	LTS	LRQ	CRD	DAGP	DBMR
Average	0.834	0.921	0.929	0.935	0.918	0.928
Skewness	-0.686	-1.108	-2.233	-1.866	-1.091	-0.591
Kurtosis	2.293	4.205	4.567	5.258	4.491	2.012
Rank (with average)	6	4	2	1	5	3

In this regard, the proposed approach was designed to process a unique frame without dependencies from the previous one. Thus, from all video sequences available, containing from 600 to 720 frames each corresponding to plots in the maize field of 250 and 300 m long respectively (i.e. 300 and 360 s), a first frame containing four crop rows is randomly selected among the 20 first frames (10 s). The images coming from the RHEA (Robotics and associated high-technologies and equipment for agriculture and forestry) project were selected under the same criteria, considering that the tractor also travelled at 3 km h⁻¹ and the image system captured frames at 10 fps.

The images were post-processed by Matlab from [MathWorks \(2015\)](#), release 8.5 (R2015a), using an Intel Core i7 2.0 GHz processor, 8 GB RAM and Windows 8.1 Pro operating system (64-bits). The proposed algorithm was developed using the graphical user interface development environment (GUIDE) incorporated into Matlab.

2.2. Image processing method architecture

The method consists of three main linked phases: (i) image segmentation, (ii) identification of starting points and (iii) crop rows detection. [Figure 3](#) shows the full structure, including the flow chart. This scheme was proposed by [García-Santillán et al. \(2017\)](#) for curved and straight crop row detection with proven validity. Image segmentation and identification of

starting points modules are preserved on this approach because of their performances, also verified on previous approaches (Section 2.3). In the proposed approach, the effort is put on a new strategy for the crop row detection module, based on the use of micro-ROIs (Location of micro-ROIs box in [Fig. 3](#)), forming a mosaic of regions that cover the full ROI. This allows to capture all information inside the micro-ROIs without the need to explore or estimate for candidate crop rows alignments (parabolas or straight lines), improving the performance of the approach by [García-Santillán et al. \(2017\)](#). Additionally, this approach improves the methods based on blobs ([Bengochea-Guevara et al., 2012; Burgos-Artizzu et al., 2011](#)) where a camera, sometimes placed on a zenithal position, captures images, which are divided into horizontal strips. For each strip, blobs of white pixels (binarised by applying the Otsu's method) are located. The central points of blobs containing a number of pixels higher than 3/4 of the height of the strip are considered as candidate to define crop rows. The method was designed to scan the binary image from top to bottom, and left to right. Afterwards, the pseudo points are removed by applying a classification algorithm and the crop rows are finally detected by least squares fitting. The algorithm was tested on more than 300 images from three image data sets, acquired from wheat, corn and soybean under different natural and field conditions. It was compared against the standard HT in terms of detection rate, accuracy and processing time. The method required about 61 ms to recognise crop rows in images of 640 × 480 pixels and the overall detection rate achieved for all 300 images was 93%. The multi-ROI approach proposed by [Jiang et al. \(2015\)](#) starts by exploring the initial central points into the ROIs (blobs), this exploration is crucial for the next central point's estimation. If this step fails, due to the presence of weeds or gaps, the method fails.

The procedure proposed in this paper was designed inspired on the above considerations. Additionally, it considers prior knowledge about crop rows detection, acquired during previous works based on blobs, and applying several constraints, also derived from previous experience. Knowledge and constraints were summarised as follows:

- In images, crops and weeds display a high degree of similarity in their spectral signatures (similar green colours), but still with sufficient differences for separation, based on image segmentation.
- A crop row in the image is an accumulation of green pixels following specific alignments (straight or curved).
- During the time of treatment in maize fields, at relatively early growth states, the weeds appear in isolated patches with respect to the crops and with irregular distributions.
- The orientation of the curved crop rows is known. Although this could be a limitation it can be solved by computing the travelling direction of the tractor based on the GPS coordinates related to the map of the plot which is to be previously stored and generally used for path planning and posterior path-following.
- In this study, assuming the x-axis of a hypothetical Cartesian co-ordinate system as the bottom part of the image, the concavity is oriented toward the left. The degree of curvature is determined by the highest quadratic polynomial degree.

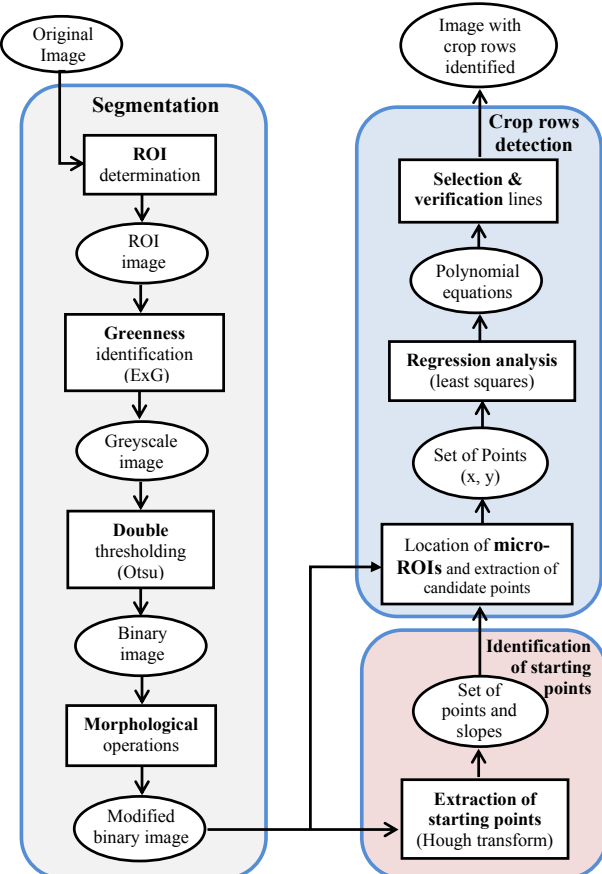


Fig. 3 – Computer vision method architecture.

- The distances of the nozzles on the maize seeder are known and fixed, producing regular inter-crop row distances, in spite of which it is assumed irregular inter-crop rows distances to assume errors during the sowing. Thus, the average crop row distances were known, assuming variations up to 200 mm if irregularities exist.
- May appear gaps along the crop rows because of the lack of seed germination, defects during sowing and other circumstances expressed above.
- The intrinsic and extrinsic parameters related to the geometry of the visual system are known.
- When there are curved crop rows, their relative initial positions on the x-axis in images change along consecutive frames due to the curvature.

The method must work under the different adverse environmental conditions expressed above.

2.3. Segmentation

Because of the need to detect curved crop rows, it is crucial to identify crop plants in order to distinguish them from weeds that also display similar spectral signatures (green colours). This is because, unlike in methods designed for straight crop rows detection, there is no prior information or applicable geometric constraints for estimating crop rows positions. Furthermore, crop rows discontinuity, together with the random distribution of weeds, reinforces the need to achieve the maximum discrimination level possible. In this regard, the automatic Otsu-based approach used by Montalvo et al. (2013), applying a double thresholding has gained in performance against other existing strategies such as the ones involving supervised learning: fuzzy clustering (Romeo et al., 2013) or support vector machines (Guerrero, Pajares, Montalvo, Romeo, & Guijarro, 2012). The supervised methods require exhaustive training, unlike the double thresholding, which has the ability to adapt to the highly changing environmental conditions common to agriculture. Under these considerations, the segmentation phase was designed with the following four linked processes: (a) ROI determination; (b) greenness identification; (c) double thresholding; and (d) morphological operations. The segmentation process produces an image where soil and green plants (crops and weeds) have been separated. The crop alignments are candidates for crop rows detection by applying curve fitting.

- ROI determination. – Defined above.
- Greenness identification. – This is carried out by applying vegetation indices, which are widely used in agriculture for identification of green plants (Burgos-Artizzu et al., 2011; Guijarro et al., 2011). In this case, given a ROI in the RGB colour space, the following normalisation scheme (Gée et al., 2008) was applied:

$$\begin{aligned} r &= \frac{R_n}{R_n + G_n + B_n}, & g &= \frac{G_n}{R_n + G_n + B_n}, \\ b &= \frac{B_n}{R_n + G_n + B_n}, \quad \text{with } r + g + b = 1 \end{aligned} \quad (1)$$

where r , g and b are the chromatic coordinates; R_n , G_n and B_n

are the normalised RGB spectral channels ranging [0, 1] and were obtained as follows:

$$R_n = \frac{R}{R_{\max}}, \quad G_n = \frac{G}{G_{\max}}, \quad B_n = \frac{B}{B_{\max}} \quad (2)$$

where R_{\max} , G_{\max} , B_{\max} are the maximum values in the corresponding spectral channels; they all usually take the maximum possible value which is 255 in 24-bit images.

The classical excess green vegetation index (ExG) given in Eq. (3) (Sogaard & Olsen, 2003; Woebbecke, Meyer, Vonbargen, & Mortensen, 1995) was selected because of its performance in agricultural images during previous experiments and after exhaustive studies with different indices (Guijarro et al., 2011) without apparent improvements. Figure 4(a) displays the ROI where ExG was applied.

$$\text{ExG} = 2g - r - b \quad (3)$$

This index is robust enough against changes in illumination conditions. Indeed, r , g and b represent relative magnitudes summing the unity. This normalisation is very useful in sensors with a unique charge-coupled device (CCD) based on

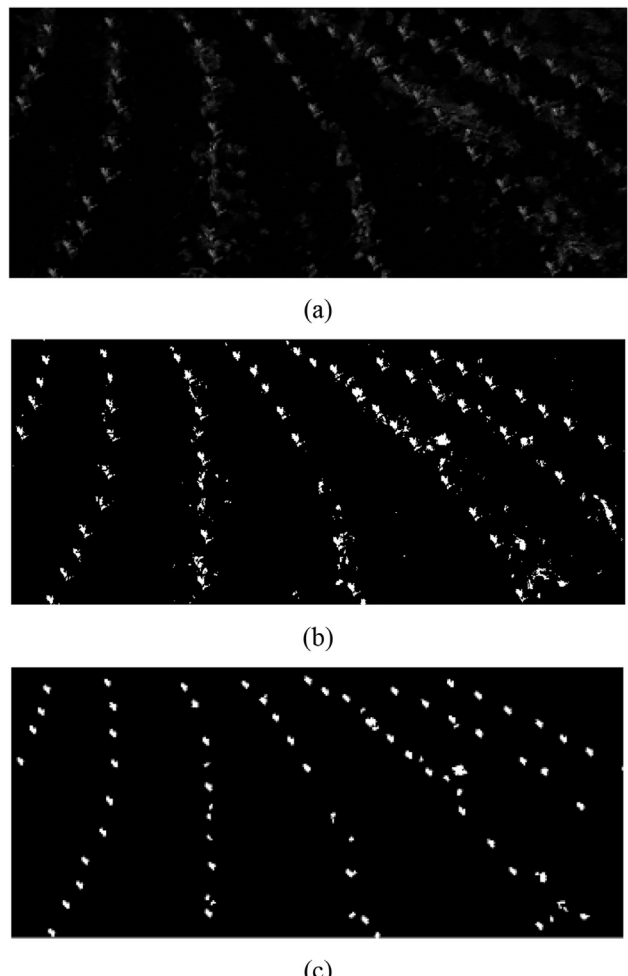


Fig. 4 – (a) Greyscale image after applying ExG; (b) binary image after applying Otsu-based double thresholding; (c) binary image after applying morphological operations.

the Bayer's filter because all cells receive an amount of radiation according to the lighting conditions, exposure time and iris aperture. The resulting colour image is obtained by interpolation preserving the relative proportion of intensities for the three Red, Green and Blue channels. So, with this normalisation the ExG obtains similar results in spite of changes in illumination, exposure time or iris aperture. During the experiments, it was verified that changes in lighting conditions, with fixed exposure time and iris aperture, did not affect the image segmentation results and consequently the final results. Nevertheless, other indices, including a combination of indices (Guizarro et al., 2011), were tested without apparent improvements. Nevertheless, the flexibility of the proposed design allows the application of any index without extra effort when required.

- c) *Double thresholding.* – Given the greyscale image after the ExG application, a first thresholding was applied to separate green plants (crops and weeds) from the soil. A second thresholding was applied over the pixels representing the green plants, which allows the partial separation between weeds and crops. Both thresholding processes were based on the Otsu's method (1979). Figure 2(b) shows the results obtained on the ROI (in the RGB colour space) with the double thresholding where soil is labelled in grey, maize plants in green and weeds in red. Figure 4(b) shows the ROI as a binary image containing a certain number of white crop rows against a black background and some isolated residual white areas belonging to weeds due to the similar spectral signatures between weeds and crops.
- d) *Morphological operations.* – Opening (Onyango & Marchant, 2003) and majority operations (in this case considering a 3×3 neighbourhood) were applied to remove insignificant small patches and spurious pixels over the binary image. A diamond-shaped structuring element for opening with a distance of 2 pixels from the origin to the vertices on the diamond sufficed. The result of this process is a binary image cleaner than the previous one, Fig. 4(c), which is the input for the next phase.

2.4. Identification of starting points

The ROI concept with sub-ROIs and the HT were applied to determine significant starting points on the basis of the ROI. The HT was used because it is a strong technique in the presence of noise or when there are hidden or incomplete parts in the image (Gonzalez, Woods, & Eddins, 2010; Pajares & De la Cruz, 2008). Astrand and Baerveldt (2005), Bakker et al. (2008) and Bakker, van Asselt, Bontsema, Muller, and van Straten (2011) verified the HT accuracy and efficiency with precision of centimetres. Nevertheless, they were exclusively designed for detecting full straight (not curved) crop rows, not to find piecewise straight rows as in the proposed approach. Its performance was also verified in terms of computational time in Han, Wang, and Kang (2012) achieving processing times less than 0.6 s.

Given the binary image, obtained in the previous phase, containing white pixels that belong to crops and weeds (some debris), a set of four starting points are identified to find the crop rows. This number is sufficient for automatic vehicle

guidance and weed identification, as justified in RHEA (2014) project. Thus, four starting points were detected as follows:

- a) The ROI was divided into two horizontal strips or sub-ROIs of equal size: top and bottom. Figure 5 shows the green dashed line which divides the ROI. The underlying idea is that with this division curved and straight crop rows can be approximated by piecewise linear segments, specifically at the bottom part of the ROI.
- b) The HT was applied to the bottom strip for identifying pixel alignments that represent the expected piecewise linear segments. It assumes some constraints by applying prior contextual knowledge to achieve maximum accuracy, namely: number of pieces of linear segments to be detected, angles of inclination in the range $[-45^\circ, 45^\circ]$, distance between the linear segments (0.85 m in the field which represented on average around 450 pixels at the bottom of the ROI). The HT was designed with resolutions of 1 pixel and 1° respectively in the accumulator space in polar coordinates.
- c) The HT uses the polar representation of the straight line defined as follows (Gonzalez & Woods, 2010):

$$\rho = x \cdot \cos \theta + y \cdot \sin \theta \quad (4)$$

where ρ is the distance of the straight line at the origin and θ is the angle that forms the normal with the x-axis. To convert the Hough parameters (ρ, θ) to the parameter space of the image (slope, intercept), the following equations were used:

$$m = -\frac{\cos \theta}{\sin \theta}, \quad d = \frac{\rho}{\sin \theta} \quad (5)$$

where m is the slope of the straight line and d is the intercept.

- d) Four peaks are identified in the Hough polar space, which determine four m and d parameters associated with four straight lines, which are drawn on the bottom strip on the ROI verifying that they cross both lower and upper edges in this sub-ROI. The four lines must contain differences in ρ greater than 300 pixels, fixed by the 0.85 m of the inter-row space with sufficient tolerance with respect to the 450 pixels. The intersection points between the detected straight lines with the lower edge in the sub-ROI determine the four starting points located at points (x, y) at the basis of the sub-ROI. Figure 5 shows four starting points, each made

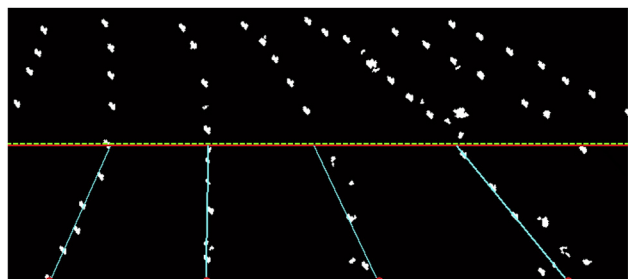


Fig. 5 – Location of starting points at the bottom strip of the ROI (up to half: green dashed line). Each starting point is made up of a crossing point (red circle) at the basis of the ROI and the slope of a straight (cyan solid line).

up of a crossing point (red circle) and the respective slope of the straight line (cyan), which indicates the initial direction to explore the crop rows.

However, high presence of weeds or large gaps can cause errors in the identification of starting points. Thus, if the number of starting points is less than four (as the number of crop rows to be detected is four), the image is rejected and then a new image is captured and processed inside the time-window of 6s. Other anomalies are also assumed by the algorithm and explained later.

2.5. Crop rows detection

At this stage, the set of four starting points are available from the previous phase, and three sequential processes are carried out for detecting the curved and straight crop rows: (a) extraction of candidate points; (b) regression analysis for fitting polynomial equations (straight/quadratic) and (c) final crop rows selection and verification.

2.5.1. Extraction of candidate points for the crop rows

The ROI is split into 12 horizontal sub-strips of equal length. This number was established after trial and error for the set of images used for experimentation. Figure 6 shows the red solid lines that divide horizontally the ROI. The lower and upper strips of the ROI contain four and eight sub-strips respectively. The different number of sub-strips was established because curved crop rows appear more pronounced at the top part and it allows capture this variability (curvature). The yellow dashed line indicates the central line of the ROI.

The crop rows are sequentially extracted from left to right (labelled 1 to 4). Each crop row is detected by exploring the sub-strips vertically, based on micro-ROIs, beginning from the associated starting point and with the slope used as guide (direction). A micro-ROI is a small rectangular region (window). The height of each micro-ROI is the same as the corresponding sub-strip. The width varies for each sub-strip being initially set to 150 pixels and decreased gradually at a rate of 5% as it progresses over the sub-strips. The initial value was established assuming that 150 pixels correspond to 0.28 m in the field over 0.85 m which is the inter-row crop space. This

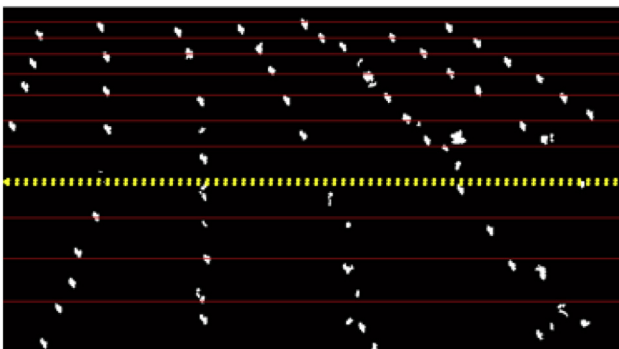


Fig. 6 – Division of the ROI into two horizontal strips of equal size (yellow dashed line): upper and lower. The lower strip is divided in four sub-strips (red solid lines) and upper strip in eight sub-strips.

size and progressive reductions guarantee that the crop rows are covered. The goal of each micro-ROI is to enclose the maximum number of crop plants leaving mostly outside the micro-ROI weeds that are located on the inter-crop row spaces. Thus, each micro-ROI is defined by four parameters [x, y, width, height], where the point (x, y) represents the upper left corner. The y, width, height are known a priori. The unknown parameter x is automatically obtained at each sub-strip. The procedure was as follows:

- 1) Place the first micro-ROI with its basis centred at the first starting point (Fig. 7a and b, red cross). Compute the geometric centre (\bar{x}, \bar{y}) of the micro-ROI as follows (Pajares & De la Cruz, 2008):

$$x_c = \frac{1}{A} \sum_i x_i; \quad y_c = \frac{1}{A} \sum_i y_i \quad (6)$$

where x_i and y_i represent the white pixels belonging to the segmented plants inside the micro-ROI; A is the number of white pixels. This expression minimises the effect of isolated pixels, Fig. 8(a). The centroid is $P_n(x_c, y_c)$ (green cross).

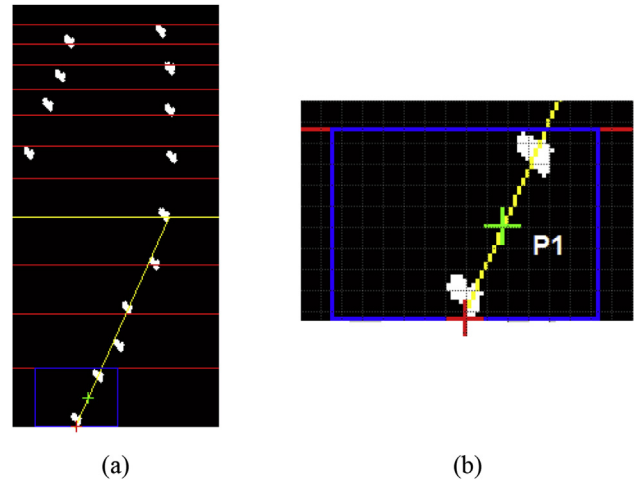


Fig. 7 – Location of micro-ROIs (blue rectangle) along the first crop row. (a) First micro-ROI located into first sub-strip; (b) Augmented micro-ROI where red cross is the lower centre of micro-ROI and green cross is the point P_1 calculated and stored.

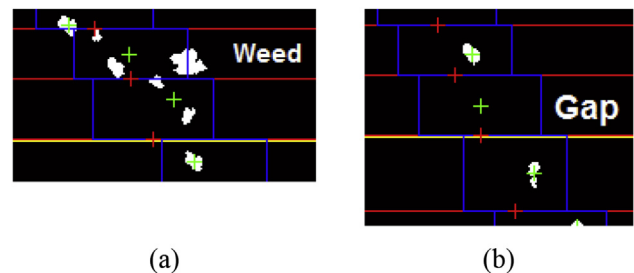
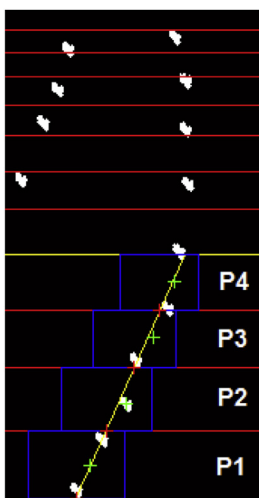


Fig. 8 – Examples of special cases. (a) Presence of weed within the micro-ROI; (b) Absence of labelled objects (gap) within the micro-ROI. Therefore, the green cross is the centroid of micro-ROI.

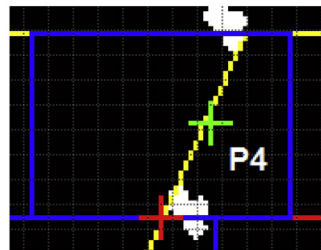
- 2) If the micro-ROI does not contain white pixels, it is considered as a gap and the point $P_n(x_c, y_c)$ is exactly the centroid of the micro-ROI as shows in Fig. 8(b). Three consecutive gaps in the same crop row are allowed at most, i.e. approximatively 1.20 m of consecutive discontinuity. Gaps with lengths greater than such discontinuities are candidates for failure, mainly on curved crop rows.
- 3) Following the estimated line with the HT associated to the first micro-ROI, three additional micro-ROIs are placed with their bases centred at the intersection points of such line with the bottom edge on the sub-strips, Fig. 9(a) and (b).
- 4) The process sketched in steps 1 to 3 is repeated for the remainder starting points, obtaining four alignments of micro-ROIs at the bottom strip with their corresponding centroids (P_n), each alignment is associated to each expected crop row to be detected.

The upper strip in the ROI, containing eight sub-strips, is explored by placing eight micro-ROIs on each expected crop row. Each micro-ROI is centred on the intersection point between the bottom edge defining the corresponding sub-strip and the straight line estimated with the previous four centroids, i.e. with the points based on the history defining the trend of the crop row. The straight line is fitted by applying least squares with the mentioned four centroids.

- 5) The fifth micro-ROI is placed, Fig. 10(a), considering the last four centroids (P_1, P_2, P_3, P_4) and the corresponding slope $m_{1,2,3,4}$ is obtained. The point of intersection (red cross in Fig. 10b) into the following sub-strip is obtained using the last centroid P_4 and the slope $m_{1,2,3,4}$.
- 6) The centroid P_5 (green cross) is calculated within this micro-ROI using Eq. (6).

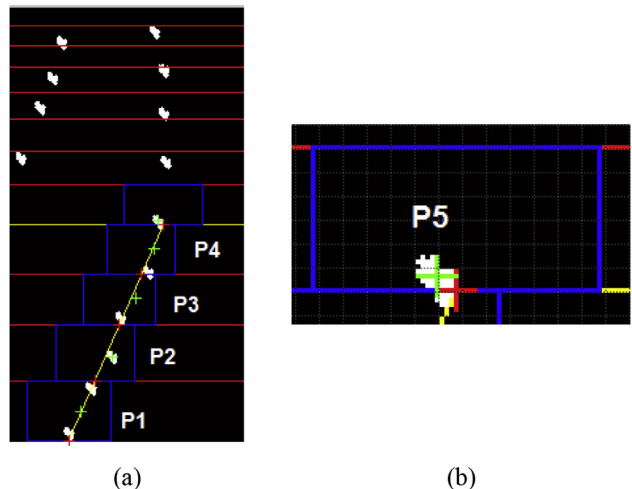


(a)

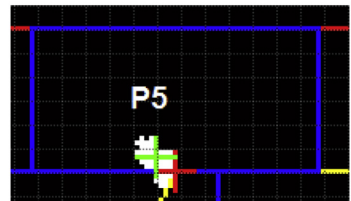


(b)

Fig. 9 – Location of micro-ROIs (blue rectangles) along the first crop row. (a) Fourth micro-ROI located into fourth sub-strip; (b) Augmented micro-ROI where red cross is on the lower centre of micro-ROI and green cross is the point P_4 calculated and stored.



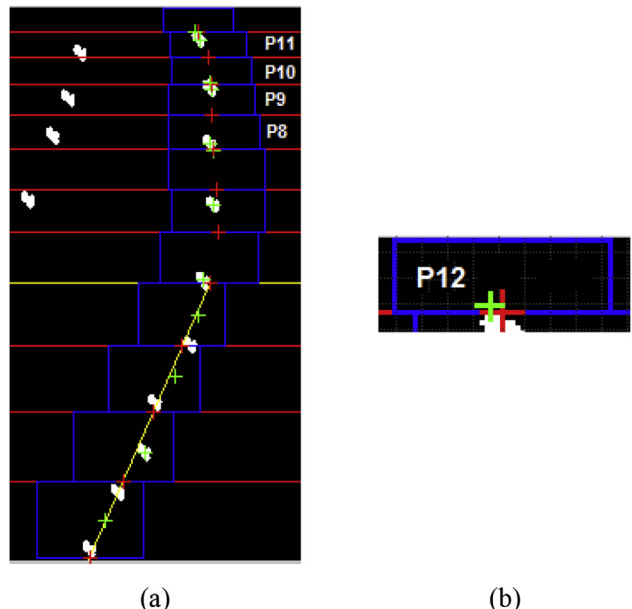
(a)



(b)

Fig. 10 – Location of micro-ROIs (blue rectangles) along the first crop row. (a) Fifth micro-ROI located into fifth sub-strip; (b) Augmented micro-ROI where red cross is the lower centre of micro-ROI and green cross is the point P_5 calculated and stored.

- 7) Steps 5 and 6 are applied for the remainder micro-ROIs within the upper strip of the ROI for the eight sub-strips associated to each expected crop row, Fig. 11(a). For instance, the centroid P_{12} , the line is fitted with the four last previous centroids (P_8, P_9, P_{10}, P_{11}) with the slope $m_{8,9,10,11}$. So, the intersection point (red cross in Fig. 11b) into the



(a)



(b)

Fig. 11 – Location of micro-ROIs (blue rectangles) along the first crop row. (a) Twelfth micro-ROI located into twelfth sub-strip; (b) Augmented micro-ROI where red cross is the lower centre of micro-ROI and green cross is the point P_{12} calculated and stored.

next sub-strip is obtained by using the previous centroid P_{11} with slope $m_{8,9,10,11}$. The centroid P_{12} (green cross) is finally obtained as above.

- 8) Once the 12 sub-strips are processed, a set of 12 points along the first crop row is obtained.

The full procedure (steps 1 to 8) is repeated for the remaining of starting points available. Figure 12 shows the result of this process. The sets of points are inputs for the next process of curve fitting by least squares.

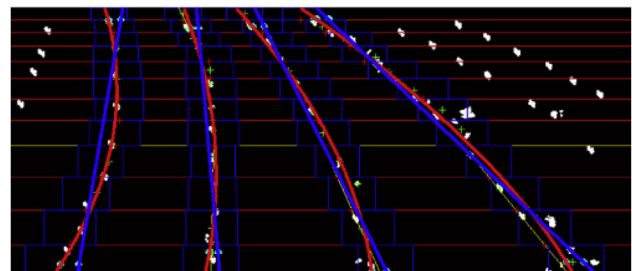
2.5.2. Regression analysis

This approach estimates the slope (m) and intercept (d) to assign an equation for a straight line ($y = mx + d$) to each crop row, usually by using least squares technique for fitting. Linear regression-based methods (Section 1.2), have been favourably tested for fitting with acceptable performances, even with low (Sogaard & Olsen, 2003) or high (Montalvo et al., 2012) weed densities. This last one achieved an efficiency rate of 95.5%. The Theil-Sen estimator (Guerrero et al., 2013) achieved up to 94.1% of efficiency rate and was robust enough even with high dispersion of pixels (weed and crop plants). Xue, Zhang, and Grift (2012) applied morphological operations and least squares for fitting, achieving an average error lower than 2.7 mm with respect the row centre-line. Based on these experiments, regression results an appropriate approach.

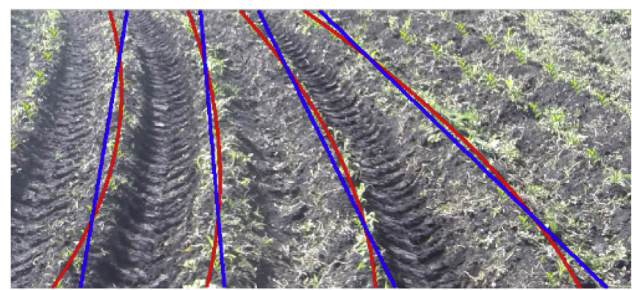
So, once the set of points, along each crop row, is obtained according to the previous process and beginning at the corresponding starting point, polynomials of degree one (straight line) and two (quadratic curve) are fitted by least squares. This technique is used to find the best-fitting curve to the available set of point by minimising the sum of the squares of the offsets of the points from the curve. For straight lines, the coefficients to be estimated are the slope (m) and the intercept (d); for the quadratic polynomial, the coefficients to be estimated are a , b and c , Eq. (7).

$$y = mx + d; \quad y = ax^2 + bx + c \quad (7)$$

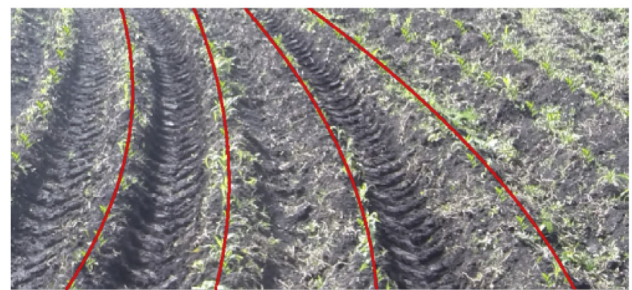
Figure 13(a) and 13(b) show the graphics of the two fitted polynomials (straight and quadratic) to each crop row of the displayed ROI. In (a) they are drawn on the binary image and in (b) on the original colour image. The straight lines appear in blue and quadratics in red. Least squares is an optimization technique to obtain a solution of an over-determined equations system, i.e. containing a greater number of equations



(a)



(b)



(c)

Fig. 13 – Graphics of the two fitted polynomials (straight and quadratic) to each crop row within the ROI. The straight lines appear in blue and quadratics in red; (a) polynomials drawn on the binary image; (b) polynomials drawn on the original colour image; (c) detected crop rows that fitted better within the ROI (curved rows).

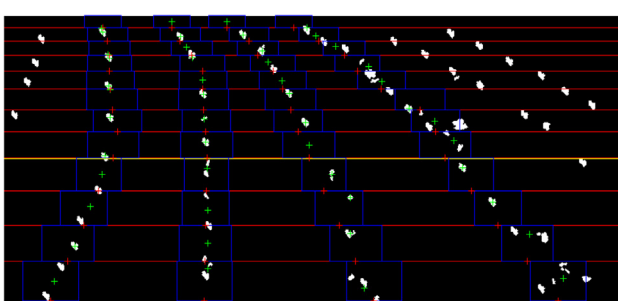


Fig. 12 – Location of micro-ROIs (blue rectangles) along the all crop row crossing by the upper and lower edges of the ROI.

than unknowns. The method finds the solution minimising the sum of squared errors between the model and data. It was computed as follows (De la Fuente & Trespaderne, 2012):

$$\min_Q \sum_{i=1}^h e_i^2(Q, Z) \quad (8)$$

where Q is the vector of parameters to be estimated, as defined in Eq. (7), Z is a vector built from the measured data, i.e. the centroids and $e_i(Q, Z)$, $i = 1, \dots, h$ a set of h equations that model the errors made when using the vector of parameters Q as a solution.

The least squares technique also gives the norm of residues as a measurement of quality of the fitting. The lower the norm, the better is the fitting. The residues are defined as the difference between the experimental values and the ones predicted by the model. The norm of residues is obtained as follows:

$$Rs = \sqrt{\sum_{i=1}^v (x_i - \hat{x}_i)^2} \quad (9)$$

where v is the number of points, x the experimental values and \hat{x} the predicted values by the model.

As a result of this process, the coefficients of the polynomials, Eq. (7), and the norm of residues, Eq. (9) are obtained. They are the inputs for the next process.

2.5.3. Final crop rows selection and verification

Two steps are applied for this process: (i) selection of rows and (ii) verification of the selected rows. In the first step, the polynomial (either straight or quadratic) that best fits each crop row is selected. The selection is carried out according to the norm of residues (Rs) obtained in the previous process, Eq. (9). The row with the least Rs value is the one selected. Figure 13(c) shows a test image with four curved crop rows selected.

In the second step, a validation of the previously selected polynomials is performed. Three cases are verified: (i) number of detected crop rows, (ii) separation between crop rows and (iii) crop row orientation.

In the first case, four crop rows should ideally be detected (1–4). This number suffices for the automatic guidance of the farming vehicle following the ideas proposed in RHEA (2014) project. If the number is lower than four, the whole image is rejected and a new image is used for the next process, otherwise it is accepted. An image can be discarded during the detection process at two stages: (a) at the beginning, when it is not possible to identify 4 starting points (Section 2.4) within the bottom ROI (Fig. 5) or (b) at the end, when 4 crop rows are not detected within the top ROI due to large gaps (>1.20 m).

In the second case, two consecutive rows must be placed at a known distance of separation at the bottom of the ROI. A greater distance expresses some anomaly. Figure 14 (a) shows the distance between two points. Perhaps the seeds sown in the furrows have not germinated and the middle row has not been detected. Based on this assumption, the verification rule can be expressed as follows: if the distance is greater than a threshold, the whole image is rejected, otherwise it is accepted. In this study the threshold was established by experimentation to be 600 pixels.

In the third case, two detected rows should not cross each other within the ROI or when they are extended outside the bottom ROI. Figure 14 (b) displays two rows intersecting

(crossing point). This situation may appear due to the presence of large gaps and high weed pressure. The crossing point (X_{cross} , Y_{cross}) is verified by the straight rows by equating both equations. The rule is as follows: if y co-ordinate (Y_{cross}) is less or equal than zero, the whole image is accepted, otherwise rejected.

In general, if any of the previously described anomalies are present, the entire image is rejected, otherwise it is accepted. As a final result, the automatic method gives the image of maize crop with four detected curved and/or straight crop rows mathematically modelled. As noted above, this number is sufficient for automatic vehicle guidance and is also convenient to destroy weeds that are located on the inter-crop row spaces, according to the ideas of the RHEA (2014) project.

2.5.4. Crop rows curvature

Regarding left/right concavity in curved crop rows, the method was designed for curved crop rows with concavity oriented toward left, Fig. 13 (c). It is useful when the tractor is moving forward and crop rows concavity is oriented toward left. However, when the tractor comes to the end of the field and starts to move back crop rows concavity will be oriented toward right. In this case, the method works as follows:

- a) A vertical specular reflection process is applied on ROI with curved crop rows oriented toward right (Fig. 15a) obtaining a new ROI with crop rows curvature oriented toward left (Fig. 15b). Namely, last column of the ROI becomes a first one, penultimate column at the second one, antepenultimate column at the third one and so on.
- b) Crop rows are detected on curves oriented toward left by using the proposed method as explained above obtaining twelve points on each crop row (Fig. 12).
- c) A horizontal translation operation is applied to each point on curved crop rows by using Eq. (10) obtaining twelve new points for each crop row.

$$P(i,j) \xrightarrow{\text{translation}} \hat{P}(i, \text{columns} - j + 1) \quad (10)$$

where columns value represents the number of columns of the ROI ($\text{columns} = 2000$).

- d) A straight or quadratic curve is fitted by least squares (Eq. (7)) using the new translated points (\hat{P}) for each crop row. These curves are oriented toward right as expected.

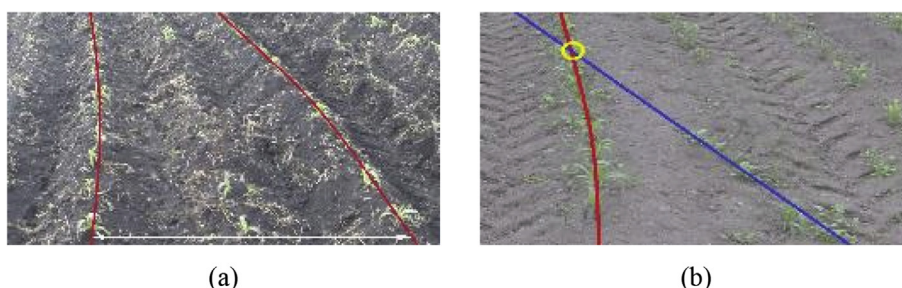


Fig. 14 – Verification process for the detected crop rows; (a) the rows are too separated due to large gaps; (b) rows intersect one another within the ROI due to high level of weed. In both cases, the whole image is rejected.

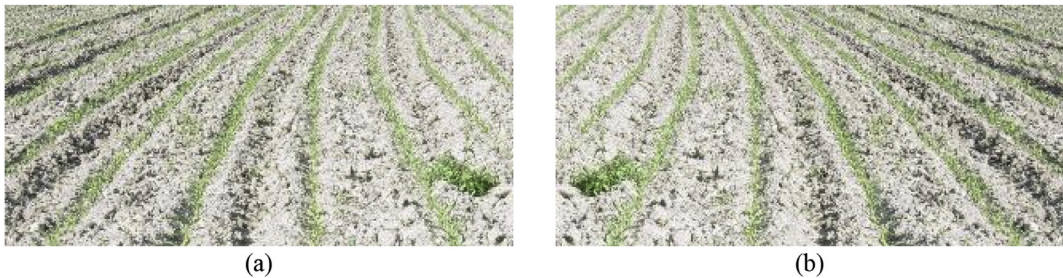


Fig. 15 – (a) Example of ROI with curved crop rows oriented toward right; (b) specular reflection with crop rows oriented toward left.

2.6. Weed infestation levels

Regarding the infestation levels, the proposed method was designed for a low level of weed coverage, according to the classification scale proposed by [Maltsev \(1962, p. 272\)](#). The percentage of weed coverage was obtained by applying the quadrant method as follows:

$$\% \text{ weed coverage} = \frac{A_{\text{weed}}}{A_{\text{sampled}}} * 100 \quad (11)$$

where A_{weed} is the area that is covered by weeds and A_{sampled} is the sampled area, i.e. $0.5 \text{ m} \times 0.5 \text{ m} = 0.25 \text{ m}^2$.

2.7. Ground truth images

The performance of the proposed method in terms of accuracy was compared to manually assessed ground truth images, which was created as follows. An expert, based on visual observation selected at least five points lying on a crop row in a test image. The coordinates of these points were relative to the upper left corner on the image. The selection was carried out considering that each point must be as close as possible to the location where the plants stalks emerge from the ground. The same procedure was carried out for the four crop rows crossing the basis of the ROI. An application developed in Matlab, based on the curve fitting toolbox, fits automatically a quadratic curve passing through these points. The selected points for crop row estimation must be sufficiently spaced, trying to cover the full crop row which is being traced, to ensure the minimum error. Sometimes, leaves of plants occlude the ideal points, especially when plant height was relatively significant. In such cases the expert places the point with the maximum accuracy as possible by observing the mapping from the 3D scene to the 2D image and the alignment of pixels on the crop rows.

A total of 920 images with plants under different growth stages (low, medium and high plant coverages, up to 40 days) were randomly selected for testing from the video sequences described in Section 2.1. The test images were divided into three sets: Set-1 containing only straight crop rows had 120 images, Set-2 containing curved crop rows equally spaced (horizontally) in 300 images and Set-3 containing curved crop rows non-equally spaced in 500 images. [Figure 16](#) shows

examples of ground truth from each test image. Set-1 from (a) to (c), Set-2 from (d) to (f) and Set-3 from (g) to (j).

3. Results and discussion

Different levels of weed infestation and gaps were considered in the sets of images. Regarding the infestation levels, the proposed method was tested with a low level of weed pressure or coverage, i.e., up to 5% of coverage according to the classification scale proposed by [Maltsev \(1962, p. 272\)](#).

Higher level of weed (>5%) could cause incorrect crop rows detection or deviations with respect the expected furrows. As mentioned before, when an incorrect detection is identified, the image is rejected, [Fig. 14\(b\)](#). Low, medium and high weed pressure in the ROI means respectively: less than 5%, between 5% and 12% and between 12% and 25%. Weed pressure above 25% led to failures with probability greater than 50%. The 5% is a limit derived from the rating scale proposed by [Maltsev \(1962, p. 272\)](#).

The coverage depended on the degree of infestation and also the plants (weeds and crops) growth state where weed and crop leaves invade the inter-crop row space, such as maize, sometimes with overlapping between weeds and crops. On average, low coverages corresponded to crop heights below 100 mm, medium between 100 and 200 mm and high between 200 and 300 mm, representing up to 40 days of growth. Crop heights greater than 300 mm can be damaged when the tractor navigates through the field with implements at the rear ([Gonzalez-de-Santos et al., 2016](#)).

In the second case, different levels of gaps were tested: low up to 0.40 m long, medium up to 0.80 m and high up to 1.20 m. Gaps greater than 1.20 m long in the same crop row were not considered because the probability of failure is greater than 50% with the camera system geometry and specifications used in the experiments, where the ROI represented 3.4 m × 5 m (width × length) at the object scale. Both, gaps and high plant coverage significantly affected the performance of the proposed method on curved and straight crop rows, mainly in the first data.

Moreover, the minimum radius of curvature of the tested curved crop rows in the experimental field was 19 m. This value was obtained by applying topographic measurements. Smaller values for the radius caused problems in the

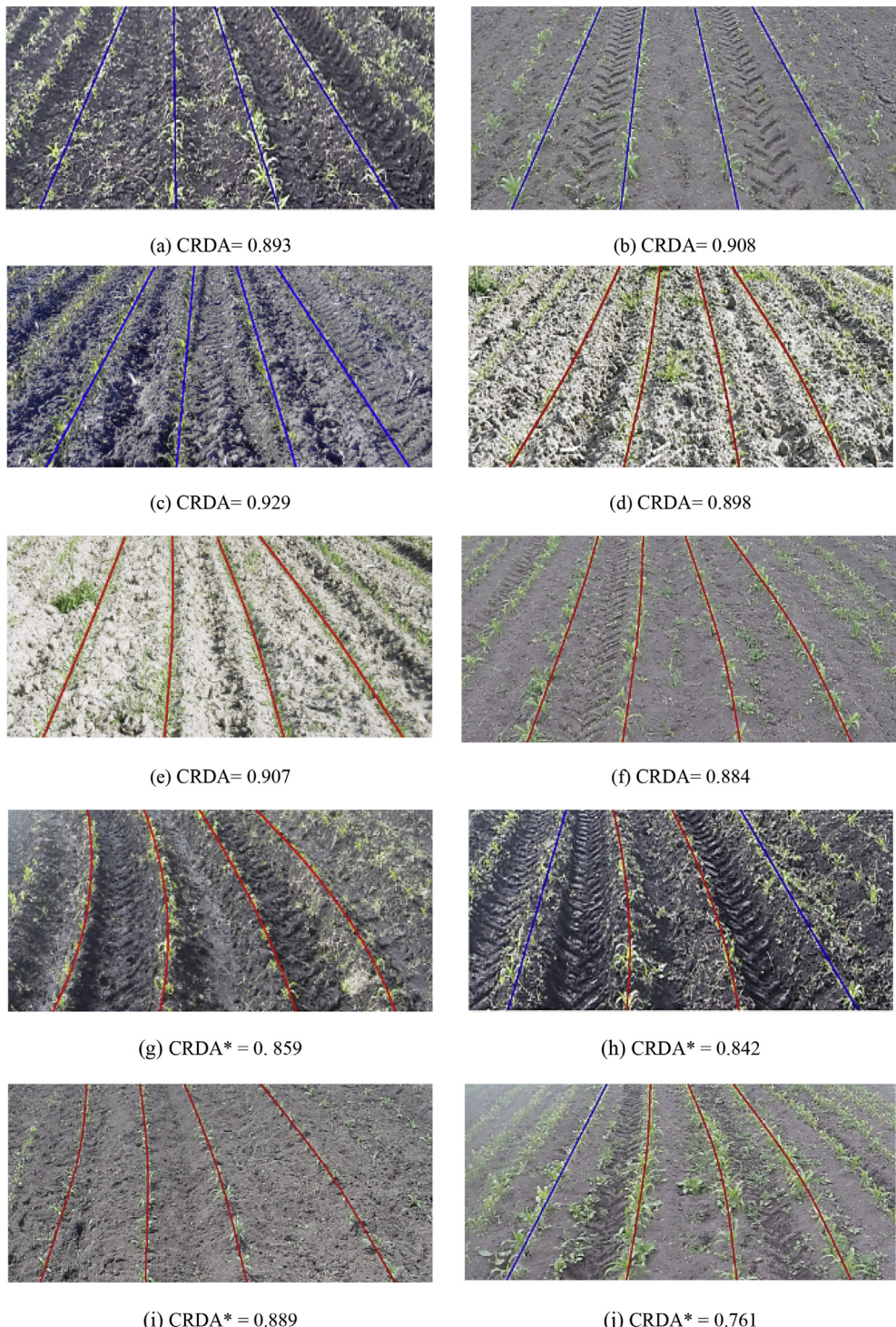


Fig. 16 – Samples of ROI for each test image set together with Crop Row Detection Accuracy (CRDA) which measures differences pixels between the estimated and expected crop rows considering the fixed inter-crop row space and the modified CRDA* which considers the maximum inter-crop row space because of the variability on the crop row separation; (a–c) Set-1 containing only straight crop rows; (d–f) Set-2 with curved crop rows equally spaced and (g–j) Set-3 with curved crop rows non-equally spaced.

navigation of the tractor and increased the risk of crop damage in the curved rows.

3.1. Comparison analysis and performance measures

Hereinafter, the proposed method for detecting both curved and straight crop rows is denoted by DBMR (Detection based on micro-ROIs). Its performance was studied based on statistical analysis and the methods used for comparison were the following: (i) Standard Hough Transform (HT) proposed by [Hough \(1962\)](#), which has been broadly used for straight crop row detection. Several constraints were applied for improving the performance of this approach, such as number of lines to be detected equal to four, the inclination angle ranging between -45° and 45° , the resolutions in distance and angle fixed to 1 pixel and 1° , respectively. (ii) Linear regression based on the Theil-Shen estimator (LTS) proposed by [Guerrero et al. \(2013\)](#) to adjust the crop rows. (iii) Linear regression based on least squares (LRQ) proposed by [Montalvo et al. \(2012\)](#), which uses templates for restricting the areas where crop rows are expected. (iv) Crop row detection (CRD) proposed by [Romeo et al. \(2012\)](#), based on image perspective projection that looks for maximum accumulation of segmented green pixels along straight alignments. (v) Template matching followed by Global Energy Minimization (TMGEM) proposed by [Vidović et al. \(2016\)](#), which detects regular patterns and uses a dynamic programming technique for determining an optimal crop model. (vi) Detection by accumulation of green pixels (DAGP), proposed by [García-Santillán et al. \(2017\)](#) to explore candidate alignments of green pixels, defining parabolas or straight lines. The HT, LTS, LRQ and CRD methods were designed for detecting straight crop rows exclusively, not for curved rows, whereas TMGEM and DAGP were designed for both curved and straight crop rows.

A measure referred as Crop Row Detection Accuracy (CRDA) was used for performance and computed by matching horizontal coordinates (x_i) for each crop row obtained by each method under evaluation (HT, LTS, LRQ, CRD, TMGEM) to the corresponding ground truth values (\hat{x}_i) according to the matching score defined by Eq. (12).

$$\text{matching_score}(\hat{x}, x, s) = \max\left(1 - \left(\frac{\hat{x} - x}{0.1*s}\right)^2, 0\right) \quad (12)$$

where s is the inter-row space in pixels for each image row.

Then the average of the matching scores for all image rows is computed, which represents a value ranging in [0, 1] and is obtained by Eq. (13). Values close to 1 determine the best performances.

$$\text{CRDA} = \frac{1}{N*M} \sum_{i=1}^M \sum_{j=1}^N \text{matching_score}(\hat{x}_{i,j}, x_{i,j}, \hat{s}_i) \quad (13)$$

where N is the number de crop rows to detect (i.e. $N = 4$), M is the number of image rows (i.e. $M = 650$).

CRDA was used for the evaluation on straight crop rows (Set-1) and curved crop rows equally spaced (Set-2). A slight variant of CRDA was proposed in this paper and used for the evaluation on curved crop rows non-equally spaced (Set-3). This new matching score is referred to as CRDA*, which uses

$\max(s)$ instead of the s value in Eq. (12). This modified score can also be used for previous test sets. However, this would imply an unnecessary extra operation (\max), increasing slightly the processing time.

3.2. Evaluation of the detection based on micro-ROIs method

The performance of the DBMR for detecting both straight and curved crop rows was evaluated through three tests (Tests 1–3). CRDA was used as the performance measure for Tests 1 and 2, while CRDA* was for Test 3. In Test 1, DBMR was compared to the HT, LTS, LRQ, CRD and DAGP on the image Set-1. In Test 2, DBMR was compared against TMGEM and DAGP on the image Set-2 and in Test 3, it was compared to the TMGEM and DAGP on the image Set-3. HT, CDR, DAGP and DBMR were implemented in Matlab, while that LTS, LRQ and TMGEM in C++. LTS and LRQ methods were implemented on a machine system, whereas the others, including the DBMR, were processed on a PC (off-line). Below the Tests 1–3 are detailed.

In Test 1, the averaged values, skewness, kurtosis and rankings of CRDA for image Set-1 are presented in [Table 1](#). Regarding the skewness, all data are skewed left because of their negative values; DBMR obtains the lower negative skewness value producing the best symmetry on the data distribution, i.e. more concentrated around the mean value. Regarding kurtosis, the shortest tail on the distribution is also obtained with DBMR. This means that the presence of outliers is minimised with a good fitting, although it achieves the third rank position with respect to the averaged values. DBMR outperforms HT and LTS on averaged values. LRQ and CRD obtain average values at the same order of magnitude than DBMR, but with worse symmetries and a greater number of outliers. HT obtains acceptable symmetries and number of outliers similar to those on DBMR, but with worse average. This means that the proposed approach is in line with well tested methods (LRD and CRD) for averaged values outperforming with respect the distribution of data (skewness and kurtosis).

In Test 2, the values of CRDA for image Set-2 are presented in [Table 2](#). As in Test-1 all data are skewed left (negative values). DBMR outperforms TMGEM and DAGP with the higher averaged value and the lower negative skewness value (best symmetry) and minimum number of outliers.

In Test 3, the values of CRDA* for image Set-3 are presented in [Table 3](#). Again DBMR outperforms TMGEM and DAGP on average, skewness and kurtosis.

Globally, from Tests 1–3, it can be seen that DBMR performs favourably, achieving similar or better performances than other existing strategies proposed for straight and curved crop rows detection with regular inter-crop row spacing, achieving clear improvements in fields containing furrows with irregular inter-crop row spaces. Additionally, DBMR and DAGP can detect straight and curved crop rows coexisting in the same image, unlike the other methods HT, CRD, LTS, LRQ and TMGEM. Thus, DBMR deals well for three types of crop rows alignments. Therefore, it can be concluded that the proposed method is moderately insensitive to curvature of crop rows and can detect straight and curved crop rows

equally and non-equally spaced with high accuracy in maize fields by using a vision system conveniently arranged on board of a tractor with a previous knowledge of the curvature (either toward left or right) of the crop rows. Figure 16 (a) to (j) shows illustrative examples representing 10 images from the 920 available (Sets 1–3). The computed crop rows are shown together with the CRDA and CRDA* values respectively, according to the extrinsic and intrinsic parameters of the visual system. High plant coverage affect significantly the performance (getting worse results, quantified around a 12%) of the proposed method on both curved and straight crop rows, mainly in the first ones as shown in Fig. 16 (j), where plants leaves spread and invade the inter-row space, sometimes with overlapping between weeds and crops.

As indicated above, TMGEM, DAGP and DBMR methods can detect both, curved and straight crop rows, unlike others methods HT, CRD, LTS and LRQ, which can only detect straight crop rows. TMGEM works with an a priori unknown number of crop rows and unknown field geometry, unlike other methods. However, TMGEM assumes that all crop rows are equally spaced in the field and in the image, unlike DAGP and DBMR, which also work on crop row non-equally spaced. CRD uses vanishing point concept to limit possible straight crop rows, but this is not applied in DBMR, because depending on the degree of curvature of furrows and curved crop rows may not converge toward the vanishing point in an image.

The computational cost was also obtained. Table 4 shows the averaged processing times in percentage (%) and milliseconds (ms) of the overall method as well as distinguishing between the image processing modules for the three sets of tested images. DBMR has the average total execution time of 573, 612 and 637 ms for each image set 1–3 respectively. The segmentation module consumes the 41.7% of total time, identification of starting points 8.8% and crop rows detection 49.6%.

Considering that in general, agricultural vehicles during tasks accomplishment work at speeds ranging between 3 and 6 km h⁻¹, this means that in the worst case (6 km h⁻¹), to travel the 5 m of the ROI (long) the vehicle needs 3 s, which is very superior to the 637 ms (in the worst case) required for image processing. The tests were carried out with the images previously stored and then processed off-line, not in real-time, but considering all required constraints for real-time. In this regard, during real-time processing the time required to capture the image must be added to the processing time given above.

In addition, it must be considered that the running time was measured in Matlab GUIDE using an interpreted programming language. It may decrease significantly by implementing the method by using a compiled programming language (e.g. C++), running on a real-time platform and operating system, e.g. LabView and CRIO as in the RHEA (2014) project. Under this implementation, the processing time could be reduced by about 40%, as reported in RHEA, improving considerably the execution time, which could be useful for real-time applications and it is a topic for future research.

Table 5 shows the averaged processing times in milliseconds (ms) for TMGEM, DAGP and DBMR methods. DBMR and DAGP achieved better performance than TMGEM. TMGEM worked on a small ROI resized to 320 × 240 pixels in order to

Table 5 – Average execution times in milliseconds (ms), ROI size and programming language for the TMGEM, DAGP and DBMR methods to detect both curved and straight crop rows.

Method	Processing time	ROI size (width × length)	Programming language
TMGEM	1749	320 × 240	C++
DAGP	721	2000 × 650	Matlab
DBMR	637	2000 × 650	Matlab

reduce the required computation time without significant loss of information. A higher spatial image resolution in pixels (640 × 480) increased considerably the processing times (4527 ms), even using the C++ compiled programming language. On the contrary, DAGP and DBMR were applied with larger ROIs (2000 × 650) pixels. This resolution suffices to capture curvature of curved crop rows.

3.3. Impact of crop rows curvature

The performance of the method has also been evaluated for detecting curved crop rows oriented toward right (Fig. 15a) and it was tested on 80 additional images containing straight and curved crop rows. The results obtained were similar to the already presented in Tables 2 and 3. The extra execution time required for both vertical specular reflection process and translation operations is less than 20 ms, i.e. the additional time is irrelevant and easily assumable for the method.

Table 6 shows the range of coefficients of higher degree for both types. This means that the crop rows analysed are limited to a group of straight and curved rows, defined by the parameters of the mathematical models, Eq. (7), i.e. straight rows with the slope (m) and quadratics with the coefficient of curvature (a). Thanks to this study, the limits of these parameters for each type of row have been identified. This allows an important improvement during the verification process, when the crop rows must be accepted or rejected depending on the computed values for the coefficients (m, a) being inside or outside of these ranges. Moreover, on curved crop rows, the maximum value for the coefficient $a = 0.0015$ (see Table 6) represents a curvature with radius of 19 m on the tested images as explained above. A negative value indicates a row with orientation toward left and a positive value toward right.

3.4. Additional considerations and future works

From the point of view of the implementation, some considerations are required. Regarding limitations of the DBMR, five constraints should be considered when it is applied: (i) number of crop rows to be detected, because only this number of alignments is allowed, (ii) the concavity of crop rows (either left or right) must be known a priori; (iii) the extrinsic and intrinsic camera parameters, (iv) height of crops in the range between 100 and 300 mm, so that leaves do not cover the ground and crop rows alignments can be distinguished from the ground and (v) the orientation of the crop row concavity cannot be detected by the proposed method; prior knowledge is required by considering the tractor travel direction combined with the GPS configuration.

Table 6 – Range of allowed values for the coefficients of greater degree for each crop type on straight and curved crop rows oriented toward left and right.

Type of line	Mathematical model	Coefficient of greater degree	Crop row orientation	Range of allowed values
Straight	$y = mx + d$	m	Left/Right	[−1 and 1]
Quadratic	$y = ax^2 + bx + c$	a	Left Right	[−0.0015 and 0] [0 and 0.0015]

The robustness of the DBMR was complemented by two procedures: (i) Selection and verification lines, where several anomalies can be assumed by the method, including the number of detected crop rows (Fig. 13c), the separation of the crop rows (between 75 and 95 mm, Fig. 14a) and their intersection (Fig. 14b), due to the significant presence of gaps (≤ 1.20 m) and weeds ($\leq 5\%$). (ii) Controlling the crop rows orientations and degrees of the coefficient for each type of line (m, a) as described in Table 6, values out of these limits could cause failures during the crop row detection.

In the future, improvements are still possible for identification of starting points, which represents an important step within the crop rows detection process. Curved crop rows detection with curvature oriented toward left or right without the knowledge priori would be desired. The quantification of weed pressure in the inter-row spaces following the ideas proposed in RHEA, as well as implementation of the proposed method by using a compiled programming language and a real-time platform and operating system intended for real-time applications should be suitable.

Moreover, as explained above, the procedure is proposed to work at each frame without dependences from the previous frames already processed. In this regard, it could exploit the fact that two consecutive frames, belonging to two consecutive ROIs, contain crop rows with similar orientations. So that, once four crop rows have been detected in a frame, this information can be used for guiding the detection of the four crop rows in the next frame under the assumption of minimum variations. Finally, another issue, to be considered is the use of the information provided by the GPS, as in the RHEA project, where a frame to be processed is captured after the tractor has travelled the long of the ROI based on the GPS coordinates.

4. Conclusions

The study proposes a new computer vision method to detect curved and straight crop rows in maize fields based on the ROI concept (region of interest) for initial growth stages in crops and weeds (up to 40 d, where leaves do not occlude the ground and crop row alignments can be distinguished from the ground). The method consists of three linked phases: segmentation, identification of starting points and crop rows detection, achieving similar or better performances than other existing strategies on furrows with regular inter-crop row spacing, but outperforming on rows with irregular inter-crop row spaces. The method can also detect straight and curved crop rows coexisting in the same image.

It has proven to be robust enough under uncontrolled lighting conditions (sunny, cloudy and intermediate days,

Fig. 1) by using a camera installed on the front of a tractor with image perspective projection. It has been tested successfully with plants under different growth stages (plant coverages) including weeds irregularly distributed in the inter-row spaces, as well as with incomplete rows (Fig. 16). The curved and straight crop rows are modelled mathematically by their respective equations for each line type. A Crop Row Detection Accuracy term (CRDA) was used for evaluation. Values close to unity indicate better performances. The proposed method works properly on straight crop rows (CRDA > 0.92 in Table 1), curved crop rows equally spaced (CRDA > 0.90 in Table 2) and curved crop rows non-equally spaced (CRDA* > 0.86 in Table 3) with concavity oriented toward left or right (not simultaneously, Fig. 15), in adverse and unexpected situations which could appear during the crop rows detection procedure, which are common in uncontrolled agricultural environments with acceptable results and processing times (≤ 637 ms in Table 4).

Acknowledgments

The research has been inspired and partially funded as part of the RHEA project funded by the European Union's Seventh Framework Programme [FP7/2007–2013] under Grant Agreement n° 245986 in the Theme NMP-2009-3.4-1 (Automation and robotics for sustainable crop and forestry management). Another part of the research leading to these results has been funded by Universidad Técnica del Norte (Ecuador) and Universidad Politécnica Estatal del Carchi (Ecuador). Also, thanks are due to the anonymous referees and editor for their very valuable and detailed comments and suggestions.

REFERENCES

- Astrand, B., & Baerveldt, A. J. (2005). A vision based row-following system for agricultural field machinery. *Mechatronics*, 15(2), 251–269.
- Bakker, T., van Asselt, K., Bontsema, J., Muller, J., & van Straten, G. (2011). Autonomous navigation using a robot platform in a sugar beet field. *Biosystems Engineering*, 109(4), 357–368.
- Bakker, T., Wouters, H., van Asselt, K., Bontsema, J., Tang, L., Müller, J., et al. (2008). A vision based row detection system for sugar beet. *Computer and Electronic in Agriculture*, 60, 87–95.
- Barreda, J., Ruiz, A., & Ribeiro, A. (2009). Seguimiento visual de líneas de cultivo [visual tracking of crop rows] (Thesis Master). Spain: Universidad de Murcia. Retrieved from <https://digitum.um.es/xmlui/bitstream/10201/22175/1/myPFC.pdf> (Accessed 18 January 2017).
- Bengochea-Guevara, J. M., Conesa-Muñoz, J., & Ribeiro, Á. (2012). Developing a small autonomous robot for crop inspection. In *Proc. technology, automation and precision farming. International*

- conference of agricultural engineering-CIGR-AgEng 2012: Agriculture and engineering for a healthier life.
- Bossu, J., Gée, Ch., Jones, G., & Truchetet, F. (2009). Wavelet transform to discriminate between crop and weed in perspective agronomic images. *Computers and Electronics in Agriculture*, 65, 133–143.
- Brosnan, T., & Sun, D.-W. (2002). Inspection and grading of agricultural and food products by computer vision systems -a review. *Computers and Electronics in Agriculture*, 36(2), 193–213.
- Burgos-Artizzu, X. P., Ribeiro, A., Guijarro, M., & Pajares, G. (2011). Real-time image processing for crop/weed discrimination in maize fields. *Computers and Electronics in Agriculture*, 75(2), 337–346.
- Davies, E. (2009). The application of machine vision to food and agriculture: A review. *The Imaging Science Journal*, 57(4), 197–217.
- De la Fuente, E., & Trespaderne, F. (2012). Visión artificial industrial: Procesamiento de imágenes para inspección automática y robótica [Industrial Machine Vision: Image Processing for automatic inspection and robotic]. Secretariado de publicaciones e intercambio editorial. Valladolid, Spain: Universidad de Valladolid.
- Emmi, L., Gonzalez-de-Soto, M., Pajares, G., & Gonzalez-de-Santos, P. (2014). New trends in robotics for agriculture: Integration and assessment of a real fleet of robots. *The Scientific World Journal*, 2014, 21. Article ID 404059.
- Fontaine, V., & Crowe, T. (2006). Development of line-detection algorithms for local positioning in densely seeded crops. *Canadian Biosystems Engineering*, 48, 19–29.
- García-Santillán, I., Guerrero, J. M., Montalvo, M., & Pajares, G. (2017). Curved and straight crop row detection by accumulation of green pixels from images in maize fields. *Precision Agriculture*. <http://dx.doi.org/10.1007/s11119-016-9494-1>.
- Gée, C., Bossu, J., Jones, G., & Truchetet, F. (2008). Crop/weed discrimination in perspective agronomic images. *Computers and Electronics in Agriculture*, 60(1), 49–59.
- Gonzalez-de-Santos, P., Ribeiro, A., Fernandez-Quintanilla, C., Lopez-Granados, F., Brandstetter, M., Tomic, S., et al. (2016). Fleets of robots for environmentally-safe pest control in agriculture. *Precision Agriculture*, 41. <http://dx.doi.org/10.1007/s11119-016-9476-3>.
- Gonzalez, R., & Woods, R. (2010). *Digital image processing* (3rd ed.). Upper Saddle River, N. J., USA: Pearson/Prentice Hall.
- Gonzalez, R., Woods, R., & Eddins, S. (2010). *Digital image processing using Matlab* (2nd ed.). New Delhi, USA: Tata McGraw Hill Education.
- Guerrero, J. M., Guijarro, M., Montalvo, M., Romeo, J., Emmi, L., Ribeiro, A., et al. (2013). Automatic expert system based on images for accuracy crop row detection in maize fields. *Expert Systems with Applications*, 40(2), 656–664.
- Guerrero, J. M., Pajares, G., Montalvo, M., Romeo, J., & Guijarro, M. (2012). Support vector machines for crop/weeds identification in maize fields. *Expert Systems with Applications*, 39, 11149–11155.
- Guijarro, M., Pajares, G., Riomoros, I., Herrera, P. J., Burgos-Artizzu, X. P., & Ribeiro, A. (2011). Automatic segmentation of relevant textures in agricultural images. *Computers and Electronics in Agriculture*, 75(1), 75–83.
- Hague, T., & Tillett, N. D. (2001). A bandpass filter-based approach to crop row location and tracking. *Mechatronics*, 11, 1–12.
- Hague, T., Tillett, N. D., & Wheeler, H. (2006). Automated crop and weed monitoring in widely spaced cereals. *Precision Agriculture*, 7(1), 21–32.
- Han, Y. H., Wang, Y. M., & Kang, F. (2012). Navigation line detection based on support vector machine for automatic agriculture vehicle. In *Proceedings of the International conference on automatic control and artificial intelligence (ACAI 2012)* (pp. 1381–1385).
- Hough, P.V.C. (1962). Method and means for recognizing complex patterns. US Patent Office No. 3069654.
- Jiang, G., Wang, Z., & Liu, H. (2015). Automatic detection of crop rows based on multi-ROIs. *Expert Systems with Applications*, 42(5), 2429–2441.
- Jiang, G., Wang, X., Wang, Z., & Liu, H. (2016). Wheat rows detection at the early growth stage based on Hough transform and vanishing point. *Computers and Electronics in Agriculture*, 123, 211–223.
- Kataoka, T., Kaneko, T., Okamoto, H., & Hata, S. (2003). Crop growth estimation system using machine vision. In *Proceedings of the IEEE International conference on advanced intelligent mechatronics (AIM 2003)* (pp. 1079–1083).
- Kise, M., & Zhang, Q. (2008). Development of a stereovision sensing system for 3D crop row structure mapping and tractor guidance. *Biosystems Engineering*, 101(2), 191–198.
- Leemans, V., & Destain, M. F. (2006). Line cluster detection using a variant of the Hough transform for culture row localisation. *Image and Vision Computing*, 24(5), 541–550.
- Maltsev, A. I. (1962). *Weed vegetation of the USSR and measures of its control*. Leningrad-Moscow: Selkhozizdat, (in Russian).
- MathWorks, Inc. (2015). Matlab Release 2015a. Retrieved from http://www.mathworks.com/products/new_products/release2015a.html (Accessed 18 January 2017).
- Montalvo, M., Guerrero, J. M., Romeo, J., Emmi, L., Guijarro, M., & Pajares, G. (2013). Automatic expert system for weeds/crops identification in images from maize fields. *Expert Systems with Applications*, 40(1), 75–82.
- Montalvo, M., Pajares, G., Guerrero, J. M., Romeo, J., Guijarro, M., Ribeiro, A., et al. (2012). Automatic detection of crop rows in maize fields with high weeds pressure. *Expert Systems with Applications*, 39(15), 11889–11897.
- Onyango, C. M., & Marchant, J. A. (2003). Segmentation of row crop plants from weeds using colour and morphology. *Computers and Electronics in Agriculture*, 39(3), 141–155.
- Otsu, N. (1979). Threshold selection method from gray-level histograms. *IEEE Transactions on Systems, Man and Cybernetics*, 9(1), 62–66.
- Pajares, G., & De la Cruz, J. M. (2008). *Visión por Computador. Imágenes digitales y aplicaciones* [Computer Vision. digital images and applications] (RA-MA Editorial, Madrid, Spain) (2nd ed.).
- RHEA. (2014). In P. Gonzalez-de-Santos, & A. Ribeiro (Eds.), *Proceedings of the second International conference on robotics and associated high-technologies and equipment for agriculture and forestry. New trends in mobile robotics, perception and actuation for agriculture and forestry*. Madrid-Spain: PGM. Spanish Research Council-CAR. Available on-line http://www.rhea-project.eu/Workshops/Conferences/Proceedings_RHEA_2014.pdf (Accessed 18 January 2017).
- Ribeiro, A., Fernandez-Quintanilla, C., Barroso, J., & Garcia-Alegre, M. C. (2005). Development of an image analysis system for estimation of weed pressure. In *Proceedings of the 5th European conference on precision agriculture (SECPA)* (pp. 169–174).
- Romeo, J., Pajares, G., Montalvo, M., Guerrero, J. M., Guijarro, M., & De la Cruz, J. M. (2013). A new expert system for greenness identification in agricultural images. *Expert Systems with Applications*, 40(6), 2275–2286.
- Romeo, J., Pajares, G., Montalvo, M., Guerrero, J. M., Guijarro, M., & Ribeiro, A. (2012). Crop row detection in maize fields inspired on the human visual perception. *Scientific World Journal*, 10. Article ID 484390.
- Rovira-Más, F., Zhang, Q., & Reid, J. F. (2008). Stereo vision three-dimensional terrain maps for precision agriculture. *Computers and Electronics in Agriculture*, 60(2), 133–143.
- Rovira-Más, F., Zhang, Q., Reid, J. F., & Will, J. D. (2003). Machine vision based automated tractor guidance. *International Journal Smart Engineering System Design*, 5(4), 467–480.

- Sogaard, H. T., & Olsen, H. J. (2003). Determination of crop rows by image analysis without segmentation. *Computers and Electronics in Agriculture*, 38(2), 141–158.
- Vidović, I., Cupec, R., & Hocenski, Ž. (2016). Crop row detection by global energy minimization. *Pattern Recognition*, 55, 68–86.
- Woebbecke, D. M., Meyer, G. E., Vonbargen, K., & Mortensen, D. A. (1995). Color indexes for weed identification under various soil, residue, and lighting conditions. *Transactions of the ASAE*, 38(1), 259–269.
- Xue, J., Zhang, L., & Grift, T. E. (2012). Variable field-of-view machine vision based row guidance of an agricultural robot. *Computers and Electronics in Agriculture*, 84, 85–91.